Structural Characterization of the $Sr_2Co_{0.5}Nb(Ta)_{0.5}O_4$ and $Sr_3CoNb(Ta)O_7$ Compounds

Han-Sang Cho, Ri-Zhu Yin, Kwang Hyun Ryu, and Chul Hyun Yo*

Department of Chemistry, Yonsei University, Seoul 120-749, Korea
Received October 12, 1999

The $Sr_2Co_{0.5}Nb(Ta)_{0.5}O_4$ and $Sr_3CoNb(Ta)O_7$ compounds, both with Ruddlesden-Popper structures, have been synthesized by the ceramic method at 1150 °C under atmospheric pressure. The crystallographic structure of the compounds was assigned to the tetragonal system with space group *I4/mmm* by X-ray diffraction(XRD) Rietveld refinement. The reduced lattice volume and lattice parameters increased as the Ta with 5d substitutes for the Nb with 4d in the compounds. The Co/Nb(Ta)O bond length has been determined by X-ray absorption spectroscopic(EXAFS/XANES) analysis and the XRD refinement. The CoO_6 octahedra were tetragonally distorted by elongation of Co-O bond along the c-axis. The magnetic measurement shows the compounds $Sr_2Co_{0.5}Nb(Ta)_{0.5}O_4$ and $Sr_3CoNb(Ta)O_7$ have paramagnetic properties and the Co ions with intermediate spin states between high and low spins in D_{4h} symmetry. All the compounds showed semiconducting behavior whose electrical conductivity increased with temperature up to 1000 K. The electrical conductivity increased and the activation energy for the conduction decreased as the number of perovskite layers increased in the compounds with chemical formula $A_{n+1}B_nO_{3n+1}$.

Introduction

Inorganic compounds including metal oxides have been widely applied to new materials such as electric, magnetic, and optical devices. To design and synthesize new materials with the desired physical properties, various methods have been explored in the academic and industrial fields. Perovskite-related oxides with a general chemical formula $A_{n+1}B_nO_{3n+1}$ have been extensively studied due to their unique and applicable properties.[1-3] The physical properties of the metal oxides depend generally on the electronic configurations of B cation and structural configurations.[4-6] Among compounds with the general formula $A_{n+1}B_nO_{3n+1}$, the metal oxides with $n = 1$ or $n = 2$ have a two-dimensional layered structure with an anisotropic property and also different physical properties from the three-dimensional materials with $n = \infty$.[7-10]

The physical properties of the layered compounds depend on the superexchange interaction between B ions through oxygen ions within the *ab* plane since the interactions between layers along *c*-axis are very weak. The weak interlayer interactions generally result in the elongation of BO_6 octahedra along *c*-axis.[11] For $CaLaFeO_4$ and $Sr_3Ir_2O_7$ compounds with two dimensional structure, the magnetic property depends on B-B distance and B-O bond covalency within the perovskite layer.[12,13]

The average distance of Fe/Ru-O in the Sr_3FeRuO_7 and Sr_4FeRuO_8 compounds is similar to that in the three-dimensional Sr_2FeRuO_6 compound. However, the Sr_3FeRuO_7 and Sr_4FeRuO_8 compounds have tetragonal distortions of Fe/RuO_6 octahedra along *c*-axis, where as the octahedra of 3-D Sr_2FeRuO_6 compound are regular.[14] The magnetic interaction of perovskite-related compounds depends on an arrangement of the transition metal ions. The two-dimensional compounds show spin glass behavior by Fe/Ru-O-Fe/Ru-O magnetic superexchange interaction between cation and neighboring cation within the *ab*-plane.

In the present work, we synthesized perovskite-related compounds and explored the relationship of the structural change due to the dimensional change and their physical properties. The structural change of $Sr_2Co_{0.5}Nb(Ta)_{0.5}O_4$ and $Sr_3CoNb(Ta)O_7$ compounds were studied by X-ray absorption spectroscopy (XAS) as well as XRD Rietveld refinement. Physical properties such as electrical conductivity and magnetic susceptibility also were studied in accordance with structural characteristics.

Experimental Section

The compounds $Sr_2Co_{0.5}Nb(Ta)_{0.5}O_4$ and $Sr_3CoNb(Ta)O_7$ with Ruddlesden-Popper type structures were synthesized with the stoichiometric starting materials of $SrCO_3$, Co_2O_3, Nb_2O_5, and Ta_2O_5. The starting materials corresponding to each composition were mixed and pre-fired at 800 °C for 2 hours. After being well ground, the mixtures were heated at 1150 °C under atmospheric pressure for 48 hours and then quenched. The grinding and heating processes were repeated several times to obtain homogeneous solid solutions. The homogeneous uniphase of each compound was identified by X-ray diffraction analysis.

X-ray diffraction patterns for the compounds were collected by the Philips PW 1710 powder diffractometer with Ni filtered Cu K_α radiation in the range $10° \leq 2\theta \leq 100°$. The Rietveld refinements of all the compounds were carried out using DBWS-9006PC software in Cerius 2 program.

Co K-edge X-ray absorption (XANES/EXAFS) spectra were recorded at the BL3C1 beamline of the Pohang Light Source (PLS) with the ring current of 100-150 mA. Si(111) double crystal monochromator was used to tune the X-ray energy for the spectroscopic data. The energy calibration was carried out with Co-metal foil before and after measur-

ing the samples in the transmission mode. X-ray absorption fine structure (XAFS) spectra were analyzed with UWXAFS 3.0 and FEFF 6.01 code.

The electrical conductivities were measured in a temperature range of 290 to 1000 K under atmospheric pressure. From the plot of log conductivity *vs* 1000/T, the activation energy of the electrical conductivity was calculated. The magnetic susceptibilities were measured using a SQUID (superconducting quantum interference devices) magnetometer in the temperature range of 5 to 300 K. The measurements were carried out after the samples were cooled in the absence of an applied field and then cooled in a magnetic field of 6500 gauss to 5 K.

Results and Discussion

Structural refinements. Analysis of X-ray diffraction patterns confirmed that all the $Sr_2Co_{0.5}Nb(Ta)_{0.5}O_4$ and $Sr_3CoNb(Ta)O_7$ compounds were homogeneously synthesized. The XRD spectra assigned them to perovskite-related compounds with the K_2NiF_4 and Ruddlesden-Popper type tetragonal system, respectively. Rietveld-refinements for the XRD patterns were carried out using tetragonal phase with the space group of *I4/mmm* as shown in Figure 1. From the results of the refinement, the average distribution of each element and the distortion of the octahedral site in the lattice can be identified. The structural parameters determined by the Rietveld refinement for XRD patterns are listed in Table 1. The lattice parameters of the Nb-substituted compounds are smaller than those of the Ta-substituted compounds due to the smaller ionic radii of Nb. In the Table 1, the tetragonality refers to the ratio between Co/Nb(Ta)-O bond length along *c*-axis and that in *ab*-plane. The tetragonalities for Ta-substituted compounds are larger than those for Nb-substituted compounds. The parameters are closely related with the electronic configuration of the transition metal and physical properties of the compounds.

The compounds $Sr_2Co_{0.5}Nb(Ta)_{0.5}O_4$ with $n = 1$ in the general formula $A_{n+1}B_nO_{3n+1}$ consist of a rock salt (AO) layer and a perovskite (ABO_3) layer, where as the compounds $Sr_3CoNb(Ta)O_7$ with $n = 2$ consist of a rock salt layer and double perovskite layer alternately along *c*-axis. The interlayer interaction between the rock salt and the perovskite layers was much weaker than the intralayer interaction in the $Sr_2Co_{0.5}Nb(Ta)_{0.5}O_4$ and $Sr_3CoNb(Ta)O_7$ compounds. The weak interlayer interactions generally resulted in the elongation of B-O bond length in BO_6 octahedra along *c*-axis. The BO_6 octahedra of the compounds $Sr_3CoNb(Ta)O_7$ with dou-

Table 1. Rietveld analysis data of the $Sr_2Co_{0.5}Nb(Ta)_{0.5}O_4$ and $Sr_3CoNb(Ta)O_7$ compounds

Compound	$Sr_2Co_{0.5}$-$Nb_{0.5}O_4$	$Sr_2Co_{0.5}$-$Ta_{0.5}O_4$	Sr_3Co-NbO_7	Sr_3CoTaO_7
Crystal system	tetragonal (*I4/mmm*)			
Lattice parameter (Å)				
a	3.891(6)	3.897(6)	3.918(0)	3.921(7)
c	12.579(5)	12.601(7)	20.356(1)	20.362(0)
Cell volume (Å^3)	190.5	191.4	312.5	313.2
Bond length (Å) [Co/Nb(Ta)-O]				
ab plan	1.946	1.949	1.959	1.961
c axis	2.114	2.172	2.063	2.149
tetragonality (*c*/*ab*)*	1.086	1.114	1.053	1.096
Reliable R-factor				
R_p(%)	8.45	6.21	7.84	7.64
R_{wp}(%)	11.18	8.26	10.23	9.88

*The tetragonality means the ratio of the bond lengths Co/Nb(Ta)-O along *c*-axis and those in *ab*-plane.

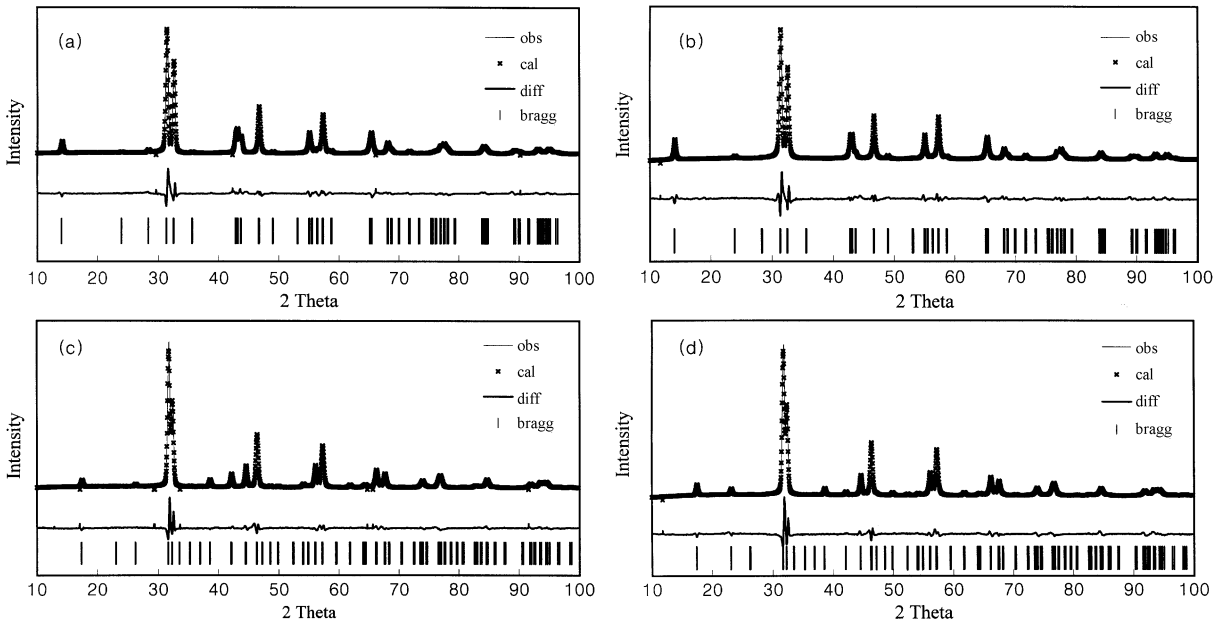

Figure 1. Rietveld refinement for XRD patterns of the (a) $Sr_2Co_{0.5}Nb_{0.5}O_4$, (b) $Sr_2Co_{0.5}Ta_{0.5}O_4$, (c) Sr_3CoNbO_7, and (d) Sr_3CoTaO_7 compounds.

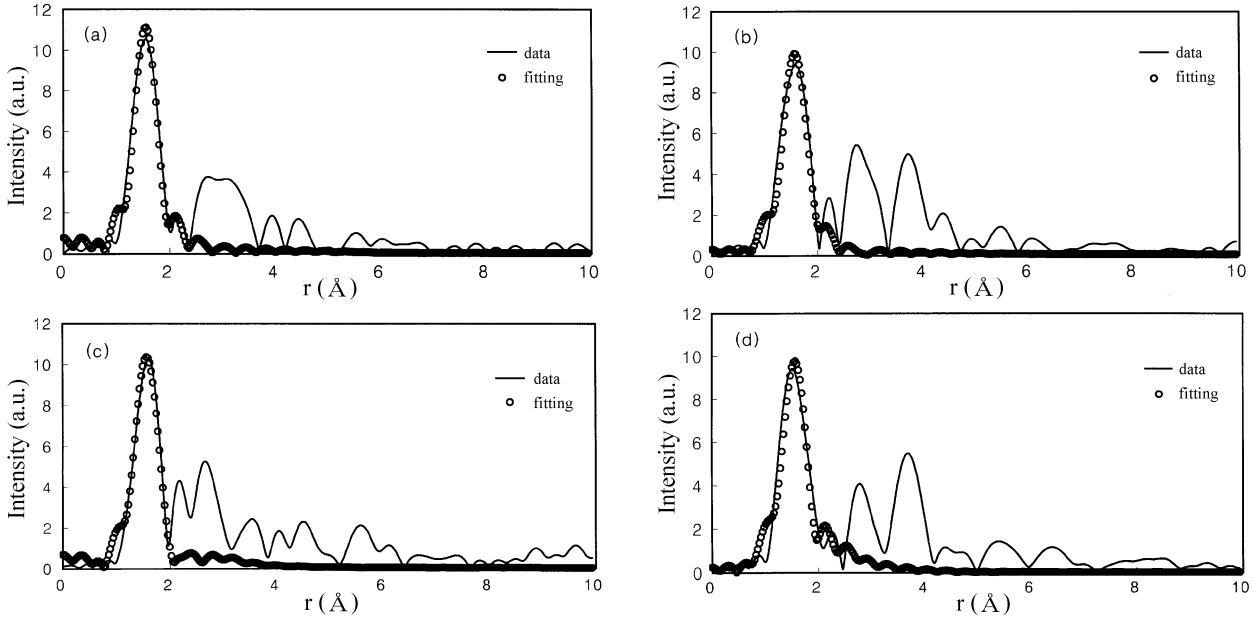

Figure 2. Co K-edge EXAFS spectra in Fourier transformed r-space of the (a) $Sr_2Co_{0.5}Nb_{0.5}O_4$, (b) $Sr_2Co_{0.5}Ta_{0.5}O_4$, (c) Sr_3CoNbO_7, and (d) Sr_3CoTaO_7 compounds.

ble perovskite layers between rock salt layers were more compressed along *c*-axis than those of $Sr_2Co_{0.5}Nb(Ta)_{0.5}O_4$.

The XRD analysis was limited on the average bulk structure because the analysis was associated with the mean structure of long-range ordering. The detailed local structure around the Co atom was studied with X-ray absorption spectroscopy. The local structures around the absorbing Co atoms were studied with the Co K-edge EXAFS spectra for the $Sr_2Co_{0.5}Nb(Ta)_{0.5}O_4$ and $Sr_3CoNb(Ta)O_7$ compounds. Figure 2 shows Fourier transforms (FT) of the k^3 weighted EXAFS spectra within the k-space range of 2.5 to 11.5 $Å^{-1}$ for the compounds. The first FT peak at ~1.7 Å corresponds to six-coordinated oxygens of the nearest neighboring atom around the absorbing Co ion. Since the scattering paths in the higher FT region are highly overlapped, separation of the FT peaks is difficult. Therefore, obtain the correct information for the local structure of the CoO_6 octahedra with two different Co-O bonds, the first Co-O path within 1-2.5 Å was considered only during fitting. On the basis of the XRD crystallographic structure, we confirmed that the first shell consists of two different Co-O bonds. When the Fourier filtered EXAFS spectra were fitted, the coordination number of Co was fixed as N=2 for Co-O bonds along *c*-axis and N=4 for those along *a,b*-axis to resolve the information of two different bonds.

Structural parameters obtained from the EXAFS refinement are listed in Table 2. For the $Sr_2Co_{0.5}Nb(Ta)_{0.5}O_4$ and $Sr_3CoNb(Ta)O_7$ compounds, differences between the Co-O bond lengths in the Nb- and Ta-substituted compounds were not significant. In contrast with the lattice parameters, the Co-O bond length was not affected by the substituted metal ions in the compounds. The tetragonalities, the ratio between Co-O bond length (*c*/*ab*), were obtained using Co K-edge EXAFS and they are listed in Table 2. The CoO_6 octahedra of the compounds $Sr_2Co_{0.5}Nb(Ta)_{0.5}O_4$ with single perovskite layers between rock salt layers were more elongated along *c*-axis than that of $Sr_3CoNb(Ta)O_7$ with double perovskite layers. Since the interlayer interactions between perovskite (ABO_3) and rock salt (AO) layers were very weak, the Co-O bonds of CoO_6 octahedra in the perovskite layer

Table 2. The bond length between atoms, Debye Waller factor, and etc. of the $Sr_2Co_{0.5}Nb(Ta)_{0.5}O_4$ and $Sr_3CoNb(Ta)O_7$ compounds

Compound	Path (Co-O)	S_0^2	N	$\sigma^2(\times10^{3\cdot*}Å^2)$	r (Å)	Tetragonality[a] (*c*-/*ab*-axes)	*R*-factor[b]
$Sr_2Co_{0.5}Nb_{0.5}O_4$	*a,b* axes	0.69	4	2.56	1.93	1.083	0.015
	c axis	0.69	2	2.71	2.09		
$Sr_2Co_{0.5}Ta_{0.5}O_4$	*a,b* axes	0.72	4	3.87	1.94	1.088	0.038
	c axis	0.72	2	4.13	2.11		
Sr_3CoNbO_7	*a,b* axes	0.76	4	3.98	1.94	1.051	0.028
	c axis	0.76	2	4.24	2.04		
Sr_3CoTaO_7	*a,b* axes	0.83	4	5.77	1.95	1.075	0.032
	c axis	0.83	2	5.79	2.10		

[a]Tetragonality means the ratio of Co-O bond lengths along *c*-axis and those along *a,b*-axis. [b]*R*-factor means the goodness of fit

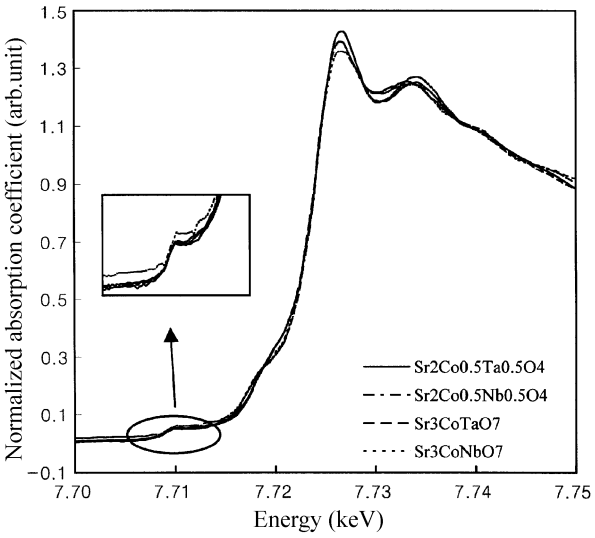

Figure 3. Co K-edge XANES spectra of the $Sr_2Co_{0.5}Nb(Ta)_{0.5}O_4$ and $Sr_3CoNb(Ta)O_7$ compounds.

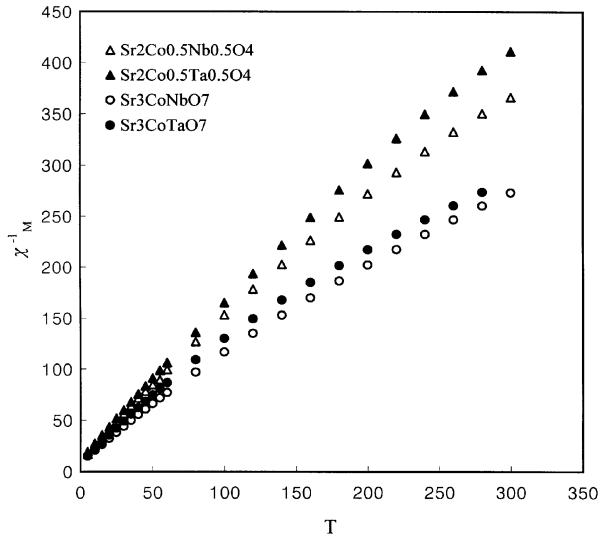

Figure 4. Plot of inverse molar magnetic susceptibility vs T for the $Sr_2Co_{0.5}Nb(Ta)_{0.5}O_4$ and $Sr_3CoNb(Ta)O_7$ compounds at the temperature range of 5 to 300 K.

were elongated along *c*-axis for the Ruddlesden-Popper type compounds. The octahedra of the compounds $Sr_2Co_{0.5}Nb(Ta)_{0.5}O_4$ were more elongated than $Sr_3CoNb(Ta)O_7$ since a perovskite layer of the former alternated with rock salt layers. As the number of rock salt layers increased in the perovskite type compounds with chemical formula $A_{n+1}B_nO_{3n+1}$, the tetragonalities of the compounds increased.

Figure 3 shows the Co K-edge normalized X-ray absorption near edge structure (XANES) for the $Sr_2Co_{0.5}Nb(Ta)_{0.5}O_4$ and $Sr_3CoNb(Ta)O_7$ compounds. The weak "pre-edge" absorption peaks at ~7707 eV correspond to the transition from 1s electron to 3d orbital. Since the transition ($\Delta l = 2$) is electric dipole forbidden in an ideal octahedral symmetry, theoretically, the pre-edge absorption should not be observed. However, the 1s $\rightarrow$ 3d transition gain some intensity in Co K-edge XANES spectra of the compounds due to electric quadruple couplings and the relative Co 3d-4p character mixing in the non-centrosymmetric environment around Co ion in distorted CoO_6 octahedral site. The $Sr_2Co_{0.5}Nb(Ta)_{0.5}O_4$ and $Sr_3CoNb(Ta)O_7$ compounds exhibits some intensity in the pre-edge region since the local structure of CoO_6 octahedra were tetragonally distorted. The main peak corresponds to the 1s $\rightarrow$ 4p transition, which is allowed by the dipolemoment. There are small shifts in the peak position, since the valence state of Co ions was same for the $Sr_2Co_{0.5}Nb(Ta)_{0.5}O_4$ and $Sr_3CoNb(Ta)O_7$ compounds.

Magnetic property. The magnetic susceptibilities for the compounds were measured in the temperature range of 5 to 300 K. The magnetic susceptibilities measured after cooling without a magnetic field are comparable to those measured after cooling with a magnetic field. The samples did not show any spin glass behavior. The inverse molar magnetic susceptibility as a function of temperature is shown in Figure 4. The compounds $Sr_2Co_{0.5}Nb(Ta)_{0.5}O_4$ and $Sr_3CoNb(Ta)O_7$ displayed paramagnetic character above 5 K. The magnetic exchange interaction was very weak since the magnetic Co ion was surrounded by non-magnetic metal ions. Therefore, there was no long-range magnetic ordering in the compounds $Sr_2Co_{0.5}Nb(Ta)_{0.5}O_4$ and $Sr_3CoNb(Ta)O_7$ above 5 K. Magnetic parameters such as the Curie constant, the paramagnetic Curie temperature, and the effective magnetic moments were estimated by Curie-Weiss law. They are listed in Table 3.

Table 3. The magnetic parameters of the $Sr_2Co_{0.5}Nb(Ta)_{0.5}O_4$ and $Sr_3CoNb(Ta)O_7$ compounds at the temperature range of 5 to 300 K

Compound	C	θ_p (°C)	μ_{eff} (B.M)
$Sr_2Co_{0.5}Nb_{0.5}O_4$	0.827	-27.5	2.57
$Sr_2Co_{0.5}Ta_{0.5}O_4$	0.735	-29.6	2.43
Sr_3CoNbO_7	1.126	-17.7	3.00
Sr_3CoTaO_7	1.051	-22.3	2.90

As shown in Table 3, the paramagnetic Curie temperature and effective magnetic moment decreased as Ta was substituted for Nb in the B site of the compounds. The effective magnetic moments depend on the electronic configurations of Co ions for the compounds $Sr_2Co_{0.5}Nb(Ta)_{0.5}O_4$ and $Sr_3CoNb(Ta)O_7$. We confirmed on the basis of the effective magnetic moments that the Co ions have an intermediate spin state between low and high spin states. Generally, Co^{3+} ions convert from low spin state to high spin state with increasing temperature. Co^{3+} ions exist with high spin state in regular octahedra of perovskite type metal oxides at room temperature.[15] However, since the CoO_6 octahedra were tetragonally distorted along *c*-axis for the compounds $Sr_2Co_{0.5}Nb(Ta)_{0.5}O_4$ and $Sr_3CoNb(Ta)O_7$, the 3d orbital of Co ions exhibited D_{4h} symmetry in tetragonal field. When the Co ion was in CoO_6 octahedra with the D_{4h} symmetry, the e_g orbital of 3d split into a_{1g} and b_{1g}. If thermal energy does not overcome the energy gap, the Co ions exist with an intermediate spin state in the two-dimensional compounds. The Co ions were in the tetragonally-distorted octahedra with intermediate spin state for the compounds $Sr_2Co_{0.5}Nb(Ta)_{0.5}O_4$ and

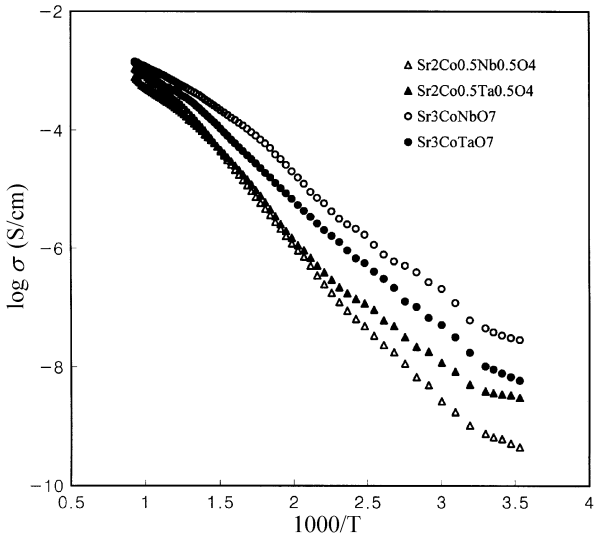

Figure 5. Plot of log electrical conductivity *vs* 1000/T for the $Sr_2Co_{0.5}Nb(Ta)_{0.5}O_4$ and $Sr_3CoNb(Ta)O_7$ compounds at the temperature range of 285 to 1073 K under the air pressure.

$Sr_3CoNb(Ta)O_7$ at room temperature. Moreover, the Ta-substituted compounds displayed smaller effective magnetic moments than Nb-substituted compounds, since the tetragonal distortion or tetragonality of the former is larger than those of the latter.

Electrical conductivity. The electrical conductivities were measured in the temperature range of 290-1000 K under atmospheric pressure. As shown in Figure 5, all the compounds exhibit the typical semiconducting property of electrical conductivity increasing with increasing temperature. The activation energy of electrical conductivities are calculated using the slope in plots of log conductivity *vs* 1000/T, and they are listed in Table 4. The electrical conductivity is described as the hopping conduction mechanism, which depends on the mobility as well as the concentration of the conduction carrier.

The conductivity of the $Sr_3CoNb(Ta)O_7$ compounds was higher than that of the $Sr_2Co_{0.5}Nb(Ta)_{0.5}O_4$ compounds. The $Sr_3CoNb(Ta)O_7$ compounds showed larger effective magnetic moments than $Sr_2Co_{0.5}Nb(Ta)_{0.5}O_4$, which was linked to the structural distortion of octahedra as described in the magnetic properties. Therefore, the $Sr_3CoNb(Ta)O_7$ compounds have higher electrical conductivities since the concentration of conduction carriers of these compounds is larger than that of the $Sr_2Co_{0.5}Nb(Ta)_{0.5}O_4$.

In addition, the $Sr_2Co_{0.5}Nb(Ta)_{0.5}O_4$ and $Sr_3CoNb(Ta)O_7$ compounds have single and double perovskite layers, respectively. Since the number of perovskite layer increases and then the mobility of the conduction carrier through the B-O-B linear bond increases in the $Sr_3CoNb(Ta)O_7$ compounds, the conductivity of these compounds is higher than that of the $Sr_2Co_{0.5}Nb(Ta)_{0.5}O_4$ compounds.[15] Finally, the electrical conductivity increased and the activation energy for the conduction decreased as the number of perovskite layers increased in the compounds with chemical formula $A_{n+1}B_nO_{3n+1}$.

Table 4. Activation energies of the electrical conductivity for the $Sr_2Co_{0.5}Nb(Ta)_{0.5}O_4$ and $Sr_3CoNb(Ta)O_7$ compounds

Compounds	Temperature range	Activation energy (eV)
$Sr_2Co_{0.5}Nb_{0.5}O_4$	290 < T < 440	0.42(8)
	440 < T < 900	0.60(9)
$Sr_2Co_{0.5}Ta_{0.5}O_4$	290 < T < 440	0.33(7)
	440 < T < 900	0.54(8)
Sr_3CoNbO_7	290 < T < 670	0.41(2)
	670 < T < 1000	0.27(2)
Sr_3CoTaO_7	290 < T < 760	0.44(2)
	760 < T < 1000	0.33(3)

Conclusion

The $Sr_2Co_{0.5}Nb(Ta)_{0.5}O_4$ and $Sr_3CoNb(Ta)O_7$ compounds with single and double perovskite layers between rock-salt layers were synthesized. Since the interactions between layers along *c*-axis were very weak in the compounds, the weak interlayer interactions generally resulted in the elongation of BO_6 octahedra along *c*-axis. As the number of perovskite layers increased in the compounds with general formula $A_{n+1}B_nO_{3n+1}$, the tetragonalities of the compounds decreased. Since the CoO_6 octahedra are tetragonally distorted along *c*-axis for the compounds $Sr_2Co_{0.5}Nb(Ta)_{0.5}O_4$ and $Sr_3CoNb(Ta)O_7$, the 3d orbital of Co ions have D_{4h} symmetry in the tetragonal system. The Co ions were in the tetragonally-distorted octahedra with an intermediate spin state for the compounds $Sr_2Co_{0.5}Nb(Ta)_{0.5}O_4$ and $Sr_3CoNb(Ta)O_7$. Since the number of perovskite layers increased and then the mobility of the conduction carrier through the B-O-B linear bond along the *ab* plane increased in the $Sr_3CoNb(Ta)O_7$ compounds, the electrical conductivity increased and the activation energy for the conduction decreased as the number of perovskite layers increased in the compounds with chemical formula $A_{n+1}B_nO_{3n+1}$.

Acknowledgment. This work was supported by project No. 96-05-01-06-01-3 of the Korean Science and Engineering Foundation for 1998 and also supported, in part, by Yonsei University Reasearch Fund for 1998. We are grateful to Pohang Light Source for the XAS measurement.

References

1. Giaquinta, D. M.; Zurloye, H. C. *Chem. Mater.* **1994**, *6*, 365.
2. Hwang, H. Y.; Cheong, S. W.; Radaelli, P. G.; Marezio, B. *Phys. Rev. Lett.* **1995**, *75*, 914.
3. Angeles, A. M.; Gomez, J.; Lopez, M. L.; Luisa, V. M. *J. Mater. Chem.* **1997**, *7*(5), 801.
4. Battle, P. D.; Jones, R. F.; Kim, S. H. *J. Mater. Chem.* **1995**, *5*, 1003.
5. Battle, P. D.; Gibb, T. C.; Herod, A. J.; Kim, S. H.; Munns, P. H. *J. Mater. Chem.* **1995**, *5*, 865.
6. Roh, K. S.; Kim, M. G.; Ryu, K. S.; Yo, C. H. *Solid State Commun.* **1996**, *100*, 565.
7. Furio, C.; Atul, P.; Nicholas, M. H.; Roberto, D.; Catlow,

C.; Richard, A. *J. Am. Chem. Soc.* **1996**, *118*, 12174.
8. Fernandez-Baca, J. A.; Wang, Z. R.; Harlow, R. L. *Phys. Rev. B* **1994**, *49*, 9198.
9. Gallagher, P. K.; Macchesney, J. B.; Bachaman, D. N. E. *J. Chem. Phys.* **1996**, *45*(7), 2466.
10. Battle, P. D.; Cox, D. E.; Green, M. A.; Millburn, J. E.; Spring, L. E.; Radaelli, P. G.; Rosseinsky, M. J.; Vente, J. F. *Chem. Mater.* **1997**, *9*, 1042.
11. Soubeyroux, J. L.; Courbin, P.; Fournes, L.; Fruchart, D. *J. Solid State Chem.* **1980**, *31*, 313.
12. Flem, G. L.; Vlasse, M.; Perrin, M. *J. Solid State Chem.* **1980**, *32*, 1.
13. Subramanian, M. A.; Crawford, M. K.; Harlow, R. L. *Mat. Res. Bull.* **1994**, *29*(6), 645.
14. Battle, P. D.; Bollen, S. K.; Powell, A. V. *J. Solid State Chem.* **1992**, *99*, 267.
15. Ryu, K. H.; Roh, K. S.; Lee, S. J.; Yo, C. H. *J. Solid State Chem.* **1993**, *105*(2), 550.